PRAMANA
— journal of
physics

Vol. 76, No. 4
April 2011
pp. 667–679

A simplified approach for the generation of projection data for cone beam geometry

TUSHAR ROY*, P S SARKAR and AMAR SINHA
Laser & Neutron Physics Section, Bhabha Atomic Research Centre, Mumbai 400 085, India
*Corresponding author. E-mail: tushar@barc.gov.in

Abstract. To test a developed reconstruction algorithm for cone beam geometry, whether it is transmission or emission tomography, one needs projection data. Generally, mathematical phantoms are generated in three dimensions and the projection for all rotation angles is calculated. For non-symmetric objects, the process is cumbersome and computation intensive. This paper describes a simple methodology for the generation of projection data for cone beam geometry for both transmission and emission tomographies by knowing the object's attenuation and/or source spatial distribution details as input. The object details such as internal geometrical distribution are nowhere involved in the projection data calculation. This simple approach uses the pixilated object matrix values in terms of the matrix indices and spatial geometrical coordinates. The projection data of some typical phantoms (generated using this approach) are reconstructed using standard FDK algorithm and Novikov's inversion formula. Correlation between the original and reconstructed images has been calculated to compare the image quality.

Keywords. Data generation; cone beam geometry; computed tomography; emission tomography.

PACS Nos 87.64.Aa; 87.59.Fm; 87.58.Ce

1. Introduction

Three-dimensional cone beam tomography [1–5] is an important tool for non-destructive examinations to look into the density distribution of an object. To execute this type of work one needs to acquire 2D projection data in cone beam geometry and then reconstruct it with proper algorithm. In this respect, the reconstruction software, being the critical part, must be tested before reconstructing actual experimental data to check its validity and determine its resolvable ability. For this very reason, projection data are obtained by performing simulated experiments using various computational techniques such as geometrical algorithms, Monte Carlo method, etc. In all these cases, the internal distribution and/or shape of the object are taken into account. For a particular angle, the projection data are calculated by finding the ray integrals along the ray path. For the next rotation angle, the projection data are calculated by first rotating the object matrix to get new object details for that angle and subsequently computing the ray integral.

2. Conventional approach for cone beam data

For symmetric objects like sphere within a sphere or coaxial cylinders, the projection data calculation is quite simple as it exploits the symmetry of the object and/or takes into account the well-defined geometry of the object. However, for objects which do not have any symmetry, the conventional methodology to calculate the projection data of a phantom for cone beam geometry in transmission and emission modes is to calculate the effective contribution which a voxel has on a ray passing from the source through a particular image pixel. This method is tedious and complex. Before presenting our approach, we discuss below the conventional method to show the computation and complexity involved.

2.1 *Transmission tomography data*

To start with a simple note, let us consider fan-beam geometry. The source is located at $S(x_c, y_c)$ and the object centred at $O(0,0)$. Let A be an $n_x \times n_y$ object matrix. For transmission case, we have

$$A\,(i,\,j) = \mu_{ij}, \quad i = 1, 2, \ldots, n_x, \quad j = 1, 2, \ldots, n_y \tag{1}$$

where μ_{ij} denotes the attenuation value at the pixel (i, j).

For a homogeneous object,

$$\mu_{ij} = \mu_0 = \text{constant}, \quad \forall i,\, j.$$

Let pixel width along X-ray direction (i.e. x-axis) is Δ. The ray passing through the object at a fan angle η is represented by $\mathbf{r}_\eta$. This ray passing through the pixel (i, j) encompasses a fraction w_{ij} of the pixel length Δ (see figures 1, 2). Hence the effective ray path in the pixel is $w_{ij}\Delta$.

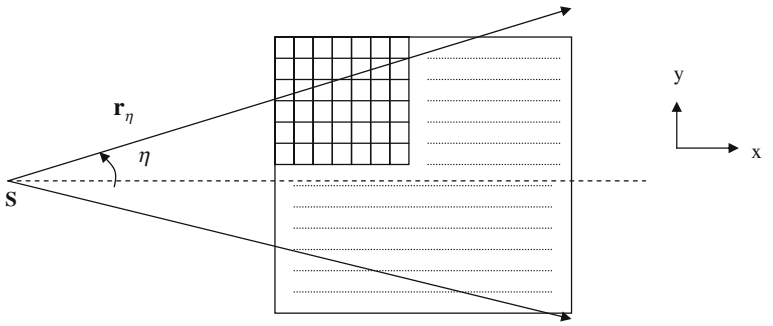

Figure 1. Fan beam geometry for transmission tomography. w_{ij}'s are calculated for all the pixels lying on the ray path $\mathbf{r}_\eta$.

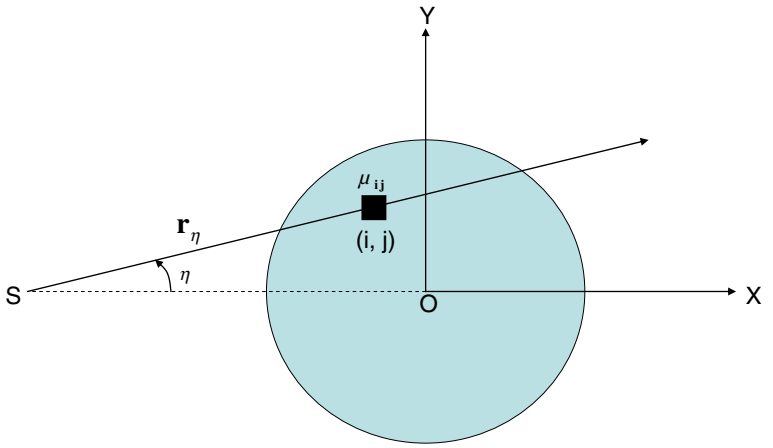

Figure 2. A ray emanating from the source S is subsequently attenuated on passing through a pixel (i, j) lying on the path $\mathbf{r}_\eta$.

The ray integral g_η is then calculated by summing the product of μ_{ij} and the effective path length $w_{ij}\Delta$ over all the pixels (i, j) lying on the ray path

$$g_\eta = \exp\left(-\Delta \sum_{\substack{(i,j)\\ \text{on } \mathbf{r}_\eta}} \mu_{ij} w_{ij}\right). \tag{2}$$

For the cone beam geometry, the procedure is similar except that in addition to the fan angle η, the cone angle φ should also be accounted for. Following the same line of argument as above, the effective ray path in the voxel (i, j, k) (in this case, voxel is to be considered instead of pixel as was the case in 2D) becomes $w_{ijk}\Delta$.

The ray integral $g_{\varphi,\eta}$ is now calculated by summing the product of μ_{ijk} and the effective path length $w_{ijk}\Delta$ over all the voxels (i, j, k) lying on the ray path

$$g_{\varphi,\eta} = \exp\left(-\Delta \sum_{\substack{(i,j,k)\\ \text{on } \mathbf{r}_{\varphi,\eta}}} \mu_{ijk} w_{ijk}\right). \tag{3}$$

2.2 *Emission tomography data*

The projection data generation in the case of emission tomography [6–8] is much more complex in the sense that the γ-ray emitted from a source point inside the object is attenuated over a part of the object, i.e. starting from the source point somewhere inside the object to its periphery.

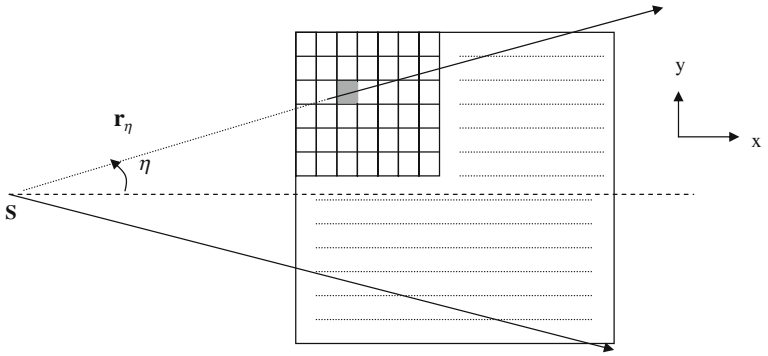

Figure 3. Fan beam geometry for emission tomography. The shaded pixel represents the source. w_{ij}'s are calculated for all the pixels lying on the ray path $\mathbf{r}_\eta$.

Consider the fan beam data collection geometry. Let $S(x_c, y_c)$ be the focal point of the fan beam. The object is centred at $O(0,0)$. Let A and F be $n_x \times n_y$ object attenuation and source matrices respectively.

$$F(i, j) = f_{ij}, \quad i = 1, 2, \ldots, n_x, \quad j = 1, 2, \ldots, n_y \tag{4}$$

and A is the same as defined in eq. (1). A photon, emitted from the pixel (i_s, j_s), passing through a point (i, j) on the path $\mathbf{r}_\eta$ encompasses a fraction w_{ij} of the pixel length Δ (see figures 3 and 4). The projection data g_η for this path is the sum of the contributions of all such source points lying on this path. Equation (2) is modified to incorporate the source term

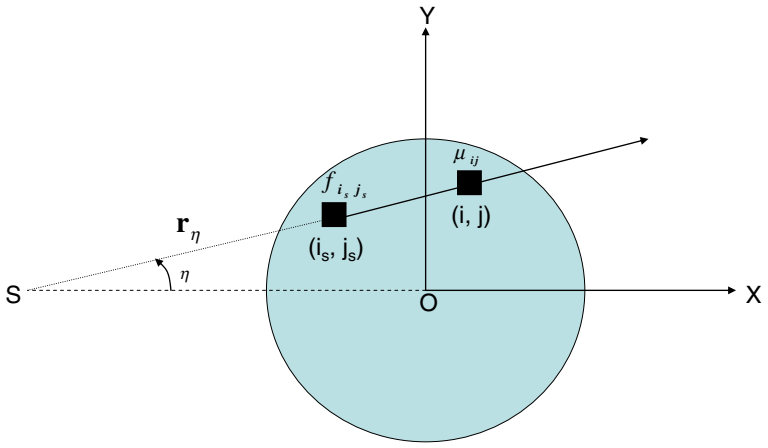

Figure 4. A ray emanating from a source pixel (i_s, j_s) is subsequently attenuated on passing through a pixel (i, j) on the path $\mathbf{r}_\eta$. The dotted line traces the ray back to the focal point S.

$$g_\eta = \sum_{\substack{(i_s,\, j_s) \\ \text{on } \mathbf{r}_\eta}} f_{i_s j_s} \exp\left(-\Delta \sum_{\substack{(i,\, j)=(n_x, n_y) \\ (i,\, j) = (i_s,\, j_s) \\ \text{on } \mathbf{r}_\eta}} \mu_{ij} w_{ij} \right), \tag{5}$$

where $f_{i_s j_s}$ is the source term at (i_s, j_s).

For cone beam data collection geometry, arguing on similar lines, the projection data $g_{\varphi,\eta}$ at cone angle φ and fan angle η is obtained by modifying eq. (3) as follows:

$$g_{\varphi,\eta} = \sum_{\substack{(i_s,\, j_s,\, k_s) \\ \text{on } \mathbf{r}_{\varphi,\eta}}} f_{i_s j_s k_s} \exp\left(-\Delta \sum_{\substack{(i,\, j,\, k)=(n_x, n_y, n_z) \\ (i,\, j,\, k) = (i_s,\, j_s,\, k_s) \\ \text{on } \mathbf{r}_{\varphi,\eta}}} \mu_{ijk} w_{ijk} \right), \tag{6}$$

where $f_{i_s j_s k_s}$ is the source term at $(i_s,\, j_s,\, k_s)$.

In this method, the crux of the problem is finding w_{ijk} or w_{ij} (as the case may be) which is tedious, time-consuming and also computation intensive. In this technique, the object matrix is re-evaluated for each projection angle separately.

3. Simpler approach for cone beam projection data

In our approach, the fraction w_{ijk} of the pixel contribution to the ray path is not calculated. The method relies on finding the coordinates of the pixels lying on the ray path and subsequently rebinning the data to find the ray integral.

3.1 *Transmission tomography projection data generation*

Let A be an $n_x \times n_y \times n_z$ object (attenuation) matrix whose elements are the attenuation values μ_{ijk}, then

$$A\,(i, j, k) = \mu_{ijk}, \quad i = 1, 2, \ldots, n_x,\ j = 1, 2, \ldots n_y,\ k = 1, 2, \ldots, n_z. \tag{7}$$

The origin $O(0, 0, 0)$ is taken to be at the centre of the object. The source is at the focal point $S\,(x_c, y_c, z_c) \equiv S\,(-D, 0, 0)$ (see figure 5). Each voxel of size Δ is represented by its index (i, j, k), coordinates (x, y, z) and μ-value (μ_{ijk}). We break the cone beam into N fans with cone angles φ (measured from the central plane $z = 0$) varying from $-\varphi_{\max}$ to $+\varphi_{\max}$ and for each cone angle φ we break the fan into N rays with fan angles η varying from $-\eta_{\max}$ to $+\eta_{\max}$. Considering object dimension of $(x_{\max}, y_{\max}, z_{\max})$

$$\varphi = \tan^{-1}\left(\frac{z}{D}\right), \quad \varphi_{\max} = \tan^{-1}\left(\frac{z_{\max}}{D}\right);$$

$$\eta = \tan^{-1}\left(\frac{y}{D}\right), \quad \eta_{\max} = \tan^{-1}\left(\frac{y_{\max}}{D}\right). \tag{8}$$

The ray passing through the object at cone angle φ and fan angle η is represented by $\mathbf{r}_{\varphi,\eta}$. The projection data for the central ray $\mathbf{r}_{0,0}$ is given by

$$g_{0,0} = \sum_{i=1}^{n_x} \mu_{ijk} \Delta = \Delta \sum_{i=1}^{n_x} \mu_{ijk}. \tag{9}$$

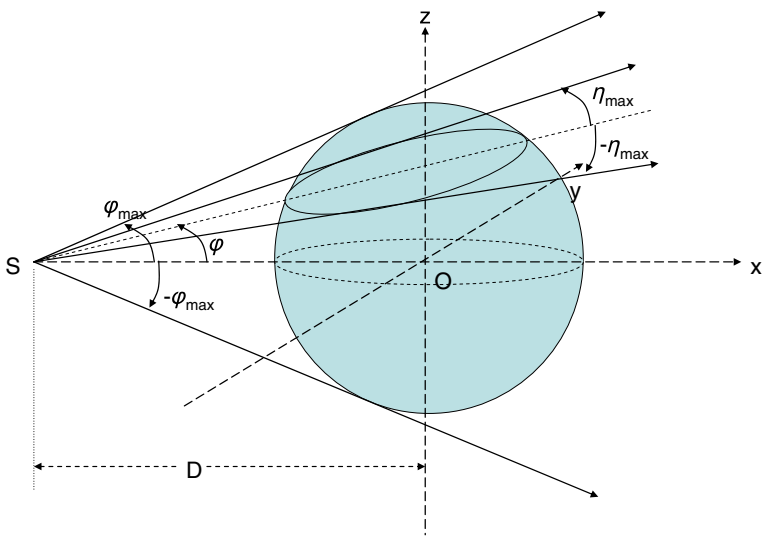

Figure 5. Cone beam geometry for data collection.

For simplicity, let us start by calculating the projection data for the central plane $z = 0$. For this plane, cone angle $\varphi = 0$ is the case for fan beam geometry. Consider the central ray $\mathbf{r}_{0,0}$. The points lying on this ray path have coordinates given by $(x, 0, 0)$. To find out the coordinates of the points on the path of the ray $\mathbf{r}_{\varphi,0}$, we rotate the frame of reference through angle φ about y-axis, the centre of rotation being $S(x_c, y_c, z_c)$. A point (x, y, z) in the original frame of reference transforms to the point (x', y', z') in the new frame of reference, where

$$\begin{aligned} x' &= (x - x_c)\cos\varphi + (z - z_c)\sin\varphi \\ y' &= y - y_c \\ z' &= -(x - x_c)\sin\varphi + (z - z_c)\cos\varphi. \end{aligned} \tag{10}$$

Two successive points lying on the path $\mathbf{r}_{0,0}$ separated by distance Δ are now separated by distance $\Delta\cos\varphi$ on the new path $\mathbf{r}_{\varphi,0}$.

Now, for the points on the ray path $\mathbf{r}_{\varphi,\eta}$, we rotate the frame of reference through angle η about z-axis, the centre of rotation being $S(x_c, y_c, z_c)$. A point (x', y', z') in the new frame of reference upon rotation through η about z-axis transforms to the point (x'', y'', z''), where

$$\begin{aligned} x'' &= x_c + \left(x'\cos\eta + y'\sin\eta\right) \\ y'' &= y_c + \left(-x'\sin\eta + y'\cos\eta\right) \\ z'' &= z_c + z'. \end{aligned} \tag{11}$$

Two successive points lying on the path $\mathbf{r}_{\varphi,0}$ separated by distance $\Delta\cos\varphi$ are now separated by distance $\Delta\cos\varphi\cos\eta$ on the new path $\mathbf{r}_{\varphi,\eta}$.

In the original frame of reference, each voxel $\Delta x \Delta y \Delta z$ located at (x, y, z) corresponds to an index (i, j, k). Now, in the rotated frame the point (x'', y'', z'') corresponds to certain index (i'', j'', k'') in the original frame of reference (see figure 6). The indices i'', j'', k'' may no longer be integers and so they are rounded off to the nearest integer under the restriction

$$1 \leq i'' \leq n_x, \quad 1 \leq j'' \leq n_y, \quad 1 \leq k'' \leq n_z.$$

The index (i'', j'', k'') will give us the μ-value at that point, $\mu_{i''j''k''}$. The projection data $g_{\varphi,\eta}$ for the ray $\mathbf{r}_{\varphi,\eta}$ will be the ray integral over all such voxels (i'', j'', k'') on this path.

$$g_{\varphi,\eta} = \Delta \cos\varphi \cos\eta \sum_{\substack{(i'', j'', k'') \\ \text{on } \mathbf{r}_{\varphi,\eta}}} \mu_{i''j''k''}. \tag{12}$$

For the projection data set at different rotation angles θ, where $0 \leq \theta \leq 2\pi$, the attenuation matrix A is first rotated through angle θ and the new attenuation matrix is obtained using bilinear interpolation. Then the above steps are performed on this rotated matrix to obtain the projection data set at angle θ.

3.2 *Emission tomography projection data generation*

Let A and F be $n_x \times n_y \times n_z$ object (attenuation) and source matrices, where

$$F(i, j, k) = f_{ijk}, \quad i = 1, 2, \ldots, n_x, \ j = 1, 2, \ldots, n_y, \ k = 1, 2, \ldots, n_z \tag{13}$$

and A is as defined in §3.1. Each voxel at (x, y, z) linked to matrix index (i, j, k) has a corresponding μ-value μ_{ijk} and a source count f_{ijk}.

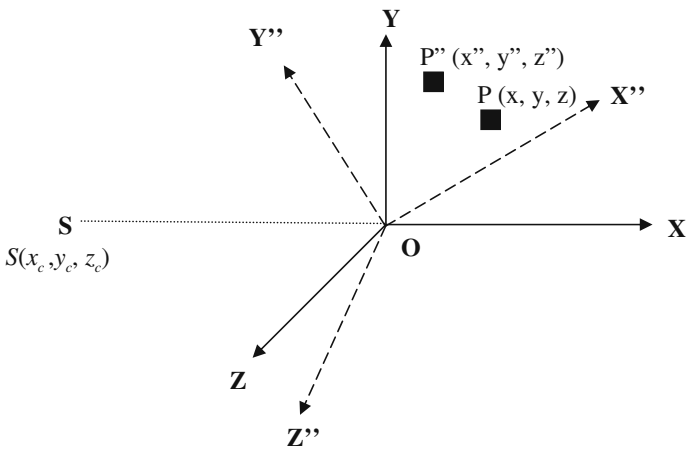

Figure 6. Transformation of a point P to P$''$ under two subsequent rotations.

The ray path through the object at cone angle φ and fan angle η is represented by $\mathbf{r}_{\varphi,\eta}$. The projection data for the central ray $\mathbf{r}_{0,0}$ are given by

$$g_{0,0} = \sum_{i_s=1}^{n_x} f_{i_s j_s k_s} \exp\left(-\Delta \sum_{i=1}^{n_x} \mu_{ijk}\right), \tag{14}$$

where $f_{i_s j_s k_s}$'s are the gamma emitting source points lying on the path $\mathbf{r}_{0,0}$.

Using similar arguments as in §3.1, point (x,y,z) transforms to (x'',y'',z'') after rotations through angle φ about y-axis and angle η about z-axis (see eqs (10) and (11)). Once the new index (i'',j'',k'') is known, we obtain the attenuation value $\mu_{i''j''k''}$ and the source value $f_{i''j''k''}$ at that point. The projection data $g_{\varphi,\eta}$ for the path $\mathbf{r}_{\varphi,\eta}$ is then given by

$$g_{\varphi,\eta} = \sum_{\substack{(i_s'', j_s'', k_s'') \\ \text{on } \mathbf{r}_{\varphi,\eta}}} f_{i_s'' j_s'' k_s''} \times \exp\left(-\Delta \cos\varphi \cos\eta \sum_{\substack{(i,j,k)=(n_x,n_y,n_z) \\ (i,j,k) = (i_s'', j_s'', k_s'') \\ \text{on } r_{\varphi,\eta}}} \mu_{i''j''k''}\right). \tag{15}$$

For the projection data set at different rotation angles θ, where $0 \leq \theta \leq 2\pi$, the attenuation matrix A and F are first rotated through angle θ and the new attenuation matrix and source matrix obtained using bilinear interpolation. Then the above steps are performed on the rotated matrices to obtain the projection data set at angle θ.

4. Reconstruction of projection data

Some mathematical phantoms, their sinograms and reconstructed images, are discussed below.

4.1 *Reconstruction of transmission projection data using FDK algorithm*

Phantom 1 consists of a solid Al cylinder ($\mu = 0.037$ mm^{-1}) of radius 10 mm and height 40 mm (figure 7a). It contains a Cu sphere ($\mu = 0.198$ mm^{-1}) of radius 2 mm centred at $(-3.2, 0, -4.2)$ and an SS rod ($\mu = 0.154$ mm^{-1}) of base radius 2 mm centred at (0, 2.8). This rod is broken from $z = -4.2$ to $z = -12$. The linear attenuation coefficient values are at 150 keV energy.

For numerical simulation purpose, Phantom 1 was discretized on a regular grid of $101 \times 101 \times 241$ units. The projections were generated for 300 views/rotations with angular step of 1.2°. D was taken as 100 mm. The reconstruction was done using FDK algorithm.

The reconstructed μ-values were found to be in the ratio 1:0.178:0.775 (Cu:Al:SS). This is in good agreement with the actual μ-value ratio 1:0.187:0.777 (Cu:Al:SS).

4.2 *Reconstruction of emission projection data using Novikov's inversion formula*

Phantom 2 represents a drum of diameter 55 cm and height 87 cm with 2 mm thick lead-lining ($\mu = 2.4588$ cm^{-1}) (figure 8a). It consists of, as shown in figure 5, a low activity

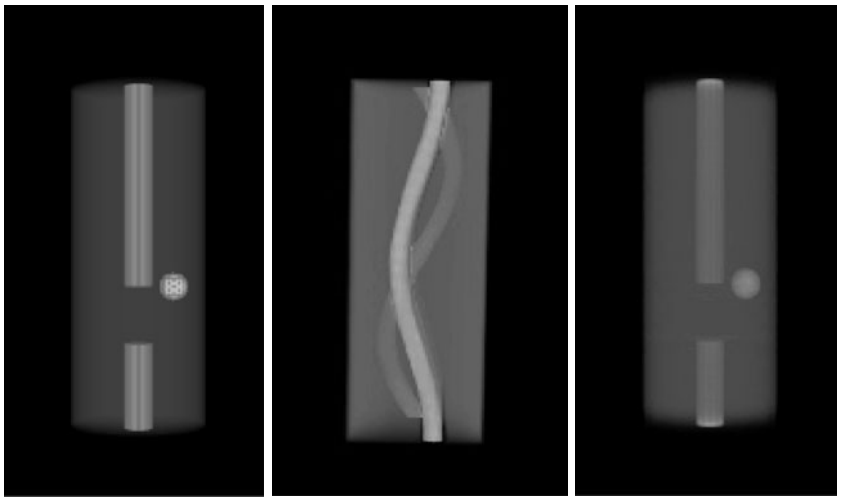

(a) (b) (c)

Figure 7. Phantom 1: (**a**) original object, (**b**) sonogram, (**c**) reconstructed object.

radioactive isotope ($\mu = 5.6311\ \text{cm}^{-1}$) in the form of small spheres at 15 different locations (refer table 1) in a surrounding matrix ($\mu = 0.12\ \text{cm}^{-1}$).

For numerical simulation purpose, Phantom 2 was discretized on a regular grid of $121 \times 121 \times 241$ units. The projections were generated for 300 views/rotations with angular step of 1.2°. The reconstruction was done using FDK-like cone-beam SPECT reconstruction algorithm [7], and D is taken as 100 cm.

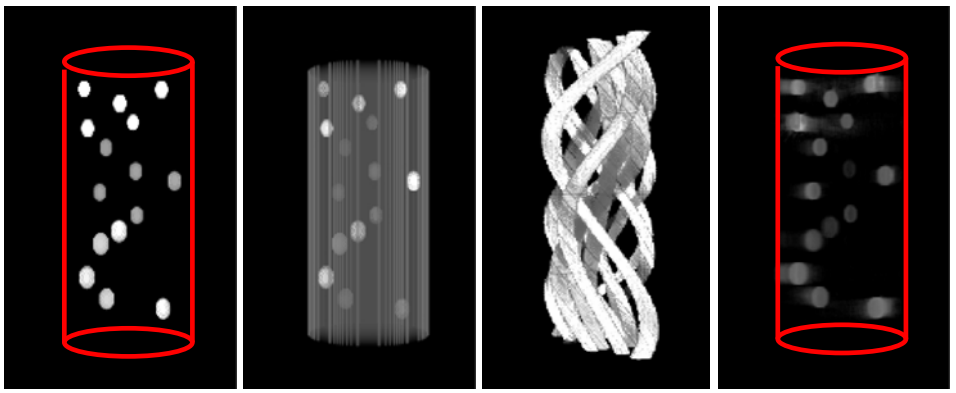

(a) (b) (c) (d)

Figure 8. Phantom 2: (**a**) activity, (**b**) attenuation map, (**c**) sinogram, (**d**) reconstructed activity. *Note:* The boundary of the drum is shown only for illustration purpose.

Table 1. Activity table for drum D-2 (central plane is the $z = 0$ plane).

Source shape/ geometry	Source position/centre (x, y, z) in cm	Source dimension (radius in cm)	Activity (counts/s)
Sphere	(15.6, −15.6, −37.5)	3.5	2×10^4
Sphere	(−11.4, −12.0, −33.7)	3.5	2×10^4
Sphere	(−19.8, 4.2, −25.0)	3.5	2×10^4
Sphere	(−13.8, −1.8, −14.1)	3.5	2×10^4
Sphere	(−5.4, 2.4, −9.8)	3.5	2×10^4
Sphere	(3.0, −15.0, −4.9)	3.0	1×10^4
Sphere	(−15.0, −18.0, 3.3)	3.0	1×10^4
Sphere	(19.2, 12.6, 6.5)	3.0	1×10^4
Sphere	(2.4, −9.0, 10.3)	3.0	1×10^4
Sphere	(−19.8, −19.2, 19.0)	3.0	1×10^4
Sphere	(−18.6, 18.0, 22.8)	2.5	3×10^4
Sphere	(1.2, −11.4, 27.2)	2.5	3×10^4
Sphere	(−4.8, 14.4, 31.0)	2.5	3×10^4
Sphere	(13.2, 19.8, 34.8)	2.5	3×10^4
Sphere	(−21.6, −5.4, 38.1)	2.5	3×10^4

5. Computation time

All the calculations were done on a standard PC with 2.4 GHz Pentium 4 processor and 1 GB RAM. For transmission, the CPU time for projection data calculation for a 121 × 121 × 241 grid was 4.33 s per projection. For emission, the CPU time for projection data calculation for a 101 × 101 × 241 grid was 4.77 s per projection.

6. Image comparison: Correlation coefficient

The correlation between the original image $g(i,j)$ and the reconstructed image $\hat{g}(i,j)$ provides a classical criterion [9]. The correlation coefficient is given by

$$\text{Correlation } (\rho) = \frac{\sum_{i=1}^{N}\sum_{j=1}^{N} g(i,j)\hat{g}(i,j)}{\sqrt{\sum_{i=1}^{N}\sum_{j=1}^{N} g(i,j)^2 \sum_{i=1}^{N}\sum_{j=1}^{N} \hat{g}(i,j)^2}}. \tag{16}$$

The correlation is equal to 1 if the images are identical, and <1 if any differences exist.

6.1 *Projection data comparison*

The main source of error in the projection data using our algorithm can be attributed to the bilinear interpolation and subsequent modification of the matrix values for each ray path. This error can be reduced by finer gridding of the data matrix at the cost of computational time.

To compare the quality of the projection data (for transmission) with the ideal data, we chose a simple object – off-centred sphere within a sphere (Phantom 3, size: 121 × 121 ×

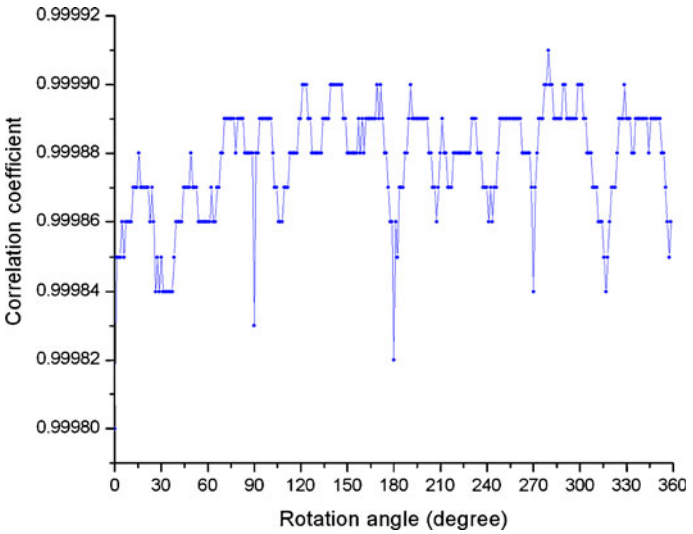

Figure 9. Plot of correlation coefficient between the projection data (for Phantom 3) computed geometrically and the projection data calculated using the algorithm) as a function of the rotation angle.

121). The ideal data were calculated geometrically by finding out the chord lengths of the X-ray passing through the object and incorporating attenuation values along its path. Figure 9 shows the plot of correlation coefficient (between the projection data as calculated geometrically and the projection data calculated using our algorithm) as a function of the rotation angle. The plot shows dips at rotation angles 90°, 180° and 270°. This is because

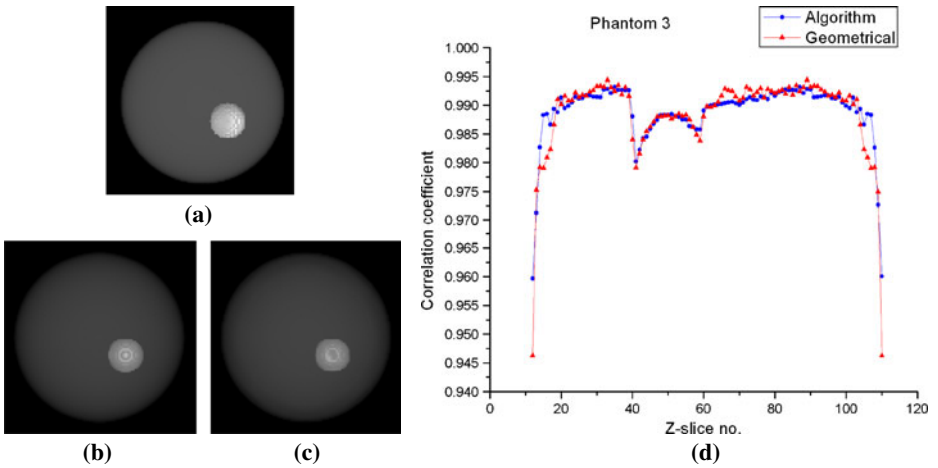

Figure 10. (**a**) Phantom 3, (**b**), (**c**) reconstructed images using projection data calculated using the algorithm and the projection data computed geometrically respectively, (**d**) plot of correlation coefficient as a function of Z-slice no.

the error due to bilinear interpolation will be maximum at 90°, 180° and 270° rotation angles.

The correlation coefficient between the two images is more than 0.99 which shows that the projection data computed by our algorithm are almost identical to those computed geometrically.

6.2 *Reconstructed image comparison*

The correlation between the reconstructed image and the original phantom has been calculated for testing the quality of the reconstructed image. Figure 10a shows the original phantom and figures 10b and c show the reconstructed images for the projection data computed using the algorithm and those computed geometrically respectively, as stated in §6.1 for Phantom 3. The correlation coefficient between the reconstructed images (figures 10b and c) and the original phantom (figure 10a) for Phantom 3 is plotted as a function of Z-slice number as shown in figure 10d.

The fluctuations in correlation coefficient in figure 10d at Z-slice nos 49 and 61 correspond to the edges of the smaller sphere. The comparatively lower correlation coefficient is due to the error introduced in the reconstruction process as they produce high-frequency component.

Figure 11 shows the plot of correlation coefficient for the Phantom 1 in §4.1. The fluctuations in correlation coefficient around Z-slices 61 and 100 correspond to the broken edges of the stainless steel rod and can be explained as before. This is evident in the sharp fall of correlation coefficient at Z-slice 61. The high-frequency component near Z-slice 100 is modified due to the presence of the copper ball and hence the fluctuations in correlation coefficient are comparatively less at Z-slice 61.

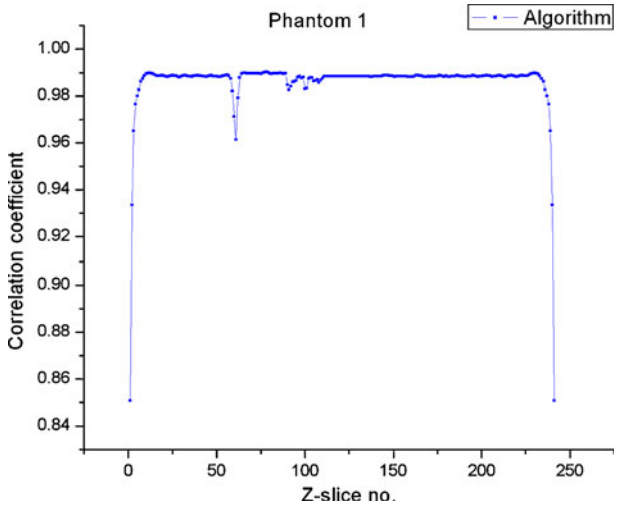

Figure 11. Plot of correlation coefficient as a function of Z-slice no. for Phantom 1.

The correlation coefficient between the reconstructed image and the original phantom is more than 0.97 and 0.98, respectively for Phantoms 3 and 1, for most of the slices. This shows a good correspondence between the original object and the reconstructed volume.

7. Conclusion

We have carried out an algorithm development study for computing the cone beam projection data for absorption-based tomography and emission tomography studies. The basis of this method lies in identifying the coordinates and the corresponding indices of the points lying on the particular ray path within the object matrix which give the corresponding μ-value and/or the source counts (for emission) in that voxel for computing the projection data.

The object information is required only as an input matrix in terms of μ and/or source terms. Nowhere the information about the geometry and shape details of the object is required in the whole calculation. The comparison of correlation coefficient shows that the reconstructed image from projection data computed by our algorithm reproduces the original phantom very well. In terms of the computing time involved, this approach may be a little slower than other faster projection data generation techniques [10] but it guarantees less complexity and easier formulation.

References

[1] F Natterer, *The mathematics of computerized tomography* (Wiley, New York, 1986)
[2] A C Kak and M Slaney, *Principles of computerized tomography* (IEEE Press, 1987)
[3] R G Novikov, *Ark. Math.* **40**, 145 (2002)
[4] L A Feldkamp, L C Davis and J W Kress, *J. Opt. Soc. Am.* **A1**, 612 (1984)
[5] P S Sarkar, A Sinha, Y Kashyap, M R More and B K Godwal, *Nucl. Instrum. Methods* **A524**, 377 (2004)
[6] F Natterer, *Inverse Problems* **17**, 113 (2001)
[7] Q Huang, G L Zeng, J You and G T Gullberg, *Phys. Med. Biol.* **50**, 2329 (2005)
[8] L A Kunyansky, *Inverse Problems* **20**, 1455 (2004)
[9] J L Starck, F Murtagh and A Bijaoui, *Image processing and data analysis* (Cambridge University Press, Cambridge, 1998) p. 287
[10] G R Davis, *Meas. Sci. Technol.* **13**, 1336 (2002)